

Synthesis and Characterization on Crystalline Structure and Magnetic Topology of $\text{Nd}_{0.75}\text{Na}_{0.25-x}\text{K}_x\text{MnO}_3$ Manganite

Tevageran Sivananthem¹, Suhadir Shamsuddin^{2*}

^{1,2*}Ceramic and Amorphous Group, Faculty of Applied Sciences and Technology, Universiti Tun Hussein Onn Malaysia, 84600 Pagoh, Johor, MALAYSIA

*Corresponding Author Designation

DOI: <https://doi.org/10.30880/ekst.2022.02.02.030>

Received 02 January 2022; Accepted 02 March 2022; Available online 23 November 2022

Abstract: The $\text{Nd}_{0.75}\text{Na}_{0.25-x}\text{K}_x\text{MnO}_3$ perovskite manganite oxide with compositions, $x = 0, 0.05$ and 0.10 respectively have been studied scientifically to untangle the effect of K substitution at the Na-site on the crystalline structure, magnetic topology, bulk density, unit cell volume and the porosity. In addition, the correlation between X-ray diffraction (XRD) measurement and Atomic Force Microscopy measurement (AFM) was also studied. In this study, a new research approach has been introduced which was revealing the magnetic topology images of the $\text{Nd}_{0.75}\text{Na}_{0.25-x}\text{K}_x\text{MnO}_3$ perovskite manganite oxide that is rarely reported by previous researchers. The samples were prepared from high purity oxide powder (99.99%) maneuvering solid state reaction method and characterized by X-ray diffraction and Atomic Force Microscopy with lift mode enabled. Furthermore, the bulk density of the samples was determined using Archimedes principle and the porosity was computed using standard formula. The AFM measurements revealed the changes occurred in magnetic domains of all the samples due to the substitution of K element. Besides that, it was also observed that the varying concentration of K substitution at the Na-site of the manganite system contributed to magnetic topology anomaly of all the samples. In addition, the XRD measurements revealed the crystalline structure of all the samples which was single phased and indexed as orthorhombic structure with *Pnma* space group. The elemental substitution had also changed the unit cell volume, bulk density, and porosity of the samples as the increase in the concentration of K element. Hence, the correlation between the XRD and AFM measurement was noticed as the results from both measurements showed good agreement.

Keywords: Crystalline Structure, Magnetic Topology, X-Ray Diffraction, Atomic Force Microscopy.

1. Introduction

The phenomena of the doped perovskite-type structure of manganese with a stoichiometric formula $\text{R}_{1-x}\text{A}_x\text{MnO}_3$ was intensively studied recently, in fundamental physics and chemistry. Whereby, R holds

the position of rare-earth based compounds such as neodymium and A stands for cation to be doped on the Mn-site of the manganite which possibly are monovalent, divalent, or trivalent [1-3]. Previous research investigated the correlation between the charge order (CO) and ferromagnetic states of $(\text{La}, \text{Nd})_{0.75}\text{Na}_{0.25}\text{MnO}_3$ manganite proposed that CO phenomenon was observed in manganite doped with univalent alkali metal cations. For $0.2 \leq x \leq 0.25$ below charge ordering temperature (T_{CO}), $\text{Pr}_{1-x}\text{Na}_x\text{MnO}_3$ is charge-ordered antiferromagnet, while $\text{Nd}_{0.75}\text{Na}_{0.25}\text{MnO}_3$ experiences a CO transition about 180 K. However, the CO characteristics of manganite doped with univalent alkali metal cations differ from those of manganite doped with divalent alkali earth cations. The author has also highlighted that $\text{La}_{0.75}\text{Na}_{0.25}\text{MnO}_3$ only suffers a transition from ferromagnetic metal to paramagnetic insulator phase between 1.8 and 400 K, whereas $\text{Nd}_{0.75}\text{Na}_{0.25}\text{MnO}_3$ suffers a charge disordered paramagnetic insulator to charge ordered paramagnetic insulator transition around 180 K [4]. Previous study done on $\text{Nd}_{0.75}\text{Na}_{0.25-x}\text{K}_x\text{MnO}_3$ exhibit results regarding the characterization of the sample, which was done on its structural analysis, observation of the surface morphology and not forgetting its electrical transportation. Through XRD analysis, it was found that all samples of the compositions are considerably in single phase, provide with no impurity peaks, and had an orthorhombic structure with a *Pnma* space group [5]. The valence state of the alkali metal ion such as K, Na, Li is +1, replacement with alkali metal at A-site can raise the valence state of Mn twice as much as alkali-earth substitution.

Besides, as a result of the substantial difference in the valence state of the La^{3+} and Li^+ , it was inferred that the generation of inhomogeneous background potential causes entrapment of electrons, which influences the creation of polarons in the metallic regime [6]. Meanwhile, if the dopant ion's ionic radius, like Ca, is the La ionic radius, it is tendency towards the *Pnma* phase in the crystal structure [7]. Numerous studies on monovalent-doped perovskite manganite still being conducted by research experts as of its properties revealed claimed to be different and special particularly $\text{Nd}_{0.75}\text{Na}_{0.25}\text{MnO}_3$ doped with cation (K^+). Although, this correlation is widely reported by numerous researchers, the significant study on topographic image of magnetic domains specifically on the $\text{Nd}_{0.75}\text{Na}_{0.25-x}\text{K}_x\text{MnO}_3$ perovskite manganite is rarely reported by previous researchers. Therefore, this study focuses on the observation of the topographic images of the magnetic domains and crystalline structure due to the substitution of K element to the $\text{Nd}_{0.75}\text{Na}_{0.25-x}\text{K}_x\text{MnO}_3$ manganite system. In this study, the sample $\text{Nd}_{0.75}\text{Na}_{0.25-x}\text{K}_x\text{MnO}_3$ ($x = 0, 0.05$ and 0.10) was prepared using solid state reaction method and characterized by X-ray diffraction and Atomic Force Microscopy with lift mode enabled which is a new field of discovery for perovskite manganite in order to investigate changes occur as the effect of K doping on the structure and magnetic topology of the samples.

2. Materials and Methods

The samples $\text{Nd}_{0.75}\text{Na}_{0.25-x}\text{K}_x\text{MnO}_3$ with $x = 0, 0.05$ and 0.10 was synthesized using solid state reaction method that involves few steps which are mixing the chemical powders (following stoichiometric formula), grinding, calcination, pelleting, and sintering. The samples were characterized by X-ray diffraction and Atomic Force Microscopy with lift mode enabled in order to study the crystalline structure and magnetic topology of the manganite samples. The density of all samples was determined using Archimedes Principle while the porosity was calculated by the standard formula from the bulk density and theoretical density. To confirm the crystalline phase of the sample, the information of values of lattice parameter and unit cell volume were analyzed through UnitCellWin software.

2.1 Chemicals and Apparatus

The chemicals that was used to prepare the samples are Neodymium (III) Oxide (Nd_2O_3), Potassium Carbonate (K_2CO_3), Sodium Carbonate (Na_2CO_3), and Manganese (IV) Oxide (MnO_2) oxide powder with high purity (99.99%). Meanwhile, the apparatus that used was high sensitivity digital electronic balance (EJ-OP-13 Density Determination Kit), agate mortar and the pestle, alumina crucible, box furnace (Protherm Furnace PLF 130/15), hydraulic press (Carver model 3851-0).

2.2 Sample preparation and characterization

The $\text{Nd}_{0.75}\text{Na}_{0.25-x}\text{K}_x\text{MnO}_3$ manganite composition of $x = 0, 0.05, \text{ and } 0.10$) was prepared using the solid-state reaction method as mentioned earlier followed by stoichiometric amounts of chemical powders with purity $\geq 99.9\%$ which are Nd_2O_3 , K_2CO_3 , Na_2CO_3 and MnO_2 . The chemical powders were carefully mixed and grinded in an agate mortar with a pestle for 2 hours. This contributes in reduction of the particle size and maximized the surface area. Through the grinding process a homogenous mixture of reactants was produced. The fine particles obtained was then calcined 2 times in air at condition of $1000\text{ }^\circ\text{C}$ for 24 hours with heating rate of $15\text{ }^\circ\text{C}/\text{min}$ to remove volatile substances, oxidizing a portion of mass, or rendering them friable. Then, it was set to be cooled at a rate of $1\text{ }^\circ\text{C}/\text{min}$. The calcined powders were then pressed using Carver hydraulic press under a load of 5 tons for 5 minutes. Through pelletizing the powders using a hydraulic press, the number of crystallites in contact was increased. The pallet produced was then sintered at temperature of $1200\text{ }^\circ\text{C}$ for 24 hours with heating rate of $15\text{ }^\circ\text{C}/\text{min}$ and was set to cool to room temperature at $1\text{ }^\circ\text{C}/\text{min}$.

The magnetic domains of the $\text{Nd}_{0.75}\text{Na}_{0.25-x}\text{K}_x\text{MnO}_3$ manganite sample was detected under the lift mode setting in Atomic Force Microscopy (Bruker) where the lift height was set at an approximate range of $1.0\text{ }\mu\text{m}$ to $10.0\text{ }\mu\text{m}$. The topographic images were generated in tapping mode using an unbiased tip (Model MESP-V2, AFM probes, Bruker Inc.) which has a nominal spring constant of 3.0 N/m . The tip possess radius of $35\mu\text{m}$ with a frequency of 75 KHz , length of $225\text{ }\mu\text{m}$ and geometry shape of rectangular. Moreover, the manufactured coating for the tip was with $0.01\text{--}0.025\text{ Ohm-cm}$ Antimony (n) doped Si. The scanning rate varied from range 0.1 to 0.6 Hz . Finally, purity of the sample prepared was examined using powder X-ray diffractometer Bruker D2 Phaser provide Cu K α radiation (1.54 \AA) at room temperature. The pellets were then grinded into powder form in and characterized using powder X-ray diffraction (XRD) Bruker D2 Phaser with the scanning rate of $2^\circ/\text{min}$ in the range of $20^\circ \leq 2\theta \leq 80^\circ$. The density of the samples was determined by Archimedes Principle and the acetone was used as buoyant medium while the porosity was calculated using standard formula.

2.3 Equations of bulk density, porosity, and theoretical density

The bulk density of the samples was determined using Archimedes principle in which the buoyant medium used was acetone. The weight of sample in air and acetone was measured using compact precision balance. Then, the bulk density was determined using Equation 1 [8].

$$\rho_{bulk} = \frac{w_{air}}{w_{air} - w_{acetone}} \times \rho_{acetone} \quad Eq.1$$

where $\rho_{acetone}$ is the density of the acetone, w_{air} is the weight of the sample in air and the $w_{acetone}$ is the weight of the sample in acetone. In the case of porosity, it was calculated by Equation 2 [8].

$$porosity\ (\%) = 1 - \frac{\rho_{bulk}}{\rho_{theoretical}} \times 100\% \quad Eq.2$$

where ρ_{bulk} is the bulk density of the sample calculated using the Equation 3.4 and $\rho_{theoretical}$ is the theoretical density calculated based on the XRD measurement using Equation 3 [8].

$$\rho_{theoretical} = \frac{n'(\sum A_c + \sum A_A)}{V_c N_A} \quad Eq.3$$

where n' is the number of formula unit, $\sum A_c$ is the sum of atomic weight of all cations, $\sum A_A$ is the sum of atomic weight of all anions, V_c is the volume of the unit cell and N_A is the Avogadro's number. The patterns of the sample will then be identified and labelled with respective miller indices (h, k, l) which indicates the Bragg's plane. The lattice parameters of a, b, c was written as shown Equation 4 [8].

$$\frac{1}{d_{hkl}^2} = \frac{h^2}{a^2} + \frac{k^2}{b^2} + \frac{l^2}{c^2} \quad Eq.4$$

where d_{hkl}^2 is the distance between the parallel plane, $h k l$ is the miller indices, and $a b c$ are lattice parameters.

3. Results and Discussion

3.1 XRD analysis

Figure 1 illustrates the structural analysis for all the $\text{Nd}_{0.75}\text{Na}_{0.25-x}\text{K}_x\text{MnO}_3$ manganite samples ($x = 0, 0.05$ and 0.10). Notably, the XRD analysis revealed that all the samples exist significantly in single phase without any impurity peaks. Hence, it was indexed as an orthorhombic structure that belongs to the $Pnma$ space group. These data correlates respectively with result reported by previous study [5,9]. The values of lattice parameter, unit cell volume, bulk density and porosity had been tabulated in Table 1. Based on the data tabulated, it can be clearly observed that the lattice parameter for all sample did not experience a systematically trend as the effect of K substitution. That being said, the values of unit cell volume (V) computed did experience a slight increase to the concentration amount of K dopant. The small increase in calculated unit cell volume (V) possibly due to the K^+ ions possess larger ionic radius ($r_{\text{K}^+} = 1.550 \text{ \AA}$) compared to substituted Na^+ ions which has smaller ionic radius ($r_{\text{Na}^+} = 1.240 \text{ \AA}$). This statement can be clearly defended by previous study which was conducted on $\text{Pr}_{0.75}\text{Na}_{0.25-x}\text{K}_x\text{MnO}_3$ and $\text{Pr}_{0.55}\text{Na}_{0.05}\text{Sr}_{0.4}\text{MnO}_3$ manganite oxide [10-11]. Besides, the modest rise in predicted unit cell volume (V) correlates well with the increasing density and decreasing porosity (P) with K content, showing a successful replacement of K^+ ions to the $\text{Nd}_{0.75}\text{Na}_{0.25-x}\text{K}_x\text{MnO}_3$ manganite oxide.

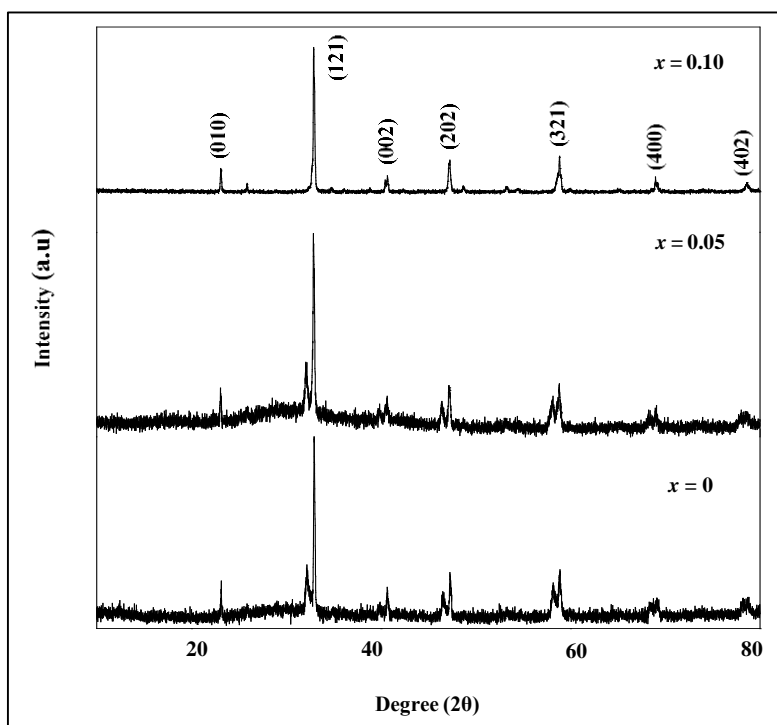


Figure 1: The X-ray Diffraction (XRD) measurement for the sample $\text{Nd}_{0.75}\text{Na}_{0.25-x}\text{K}_x\text{MnO}_3$ with $x = 0, 0.05$ and 0.10 .

Table 1: Lattice parameters, unit cell volume (V), bulk density (ρ_{bulk}) and porosity of the sample $\text{Nd}_{0.75}\text{Na}_{0.25-x}\text{K}_x\text{MnO}_3$ for compositions $x = 0, 0.05$ and 0.10 .

Sample	Lattice parameter, \AA (± 0.001)			V , \AA^3 (± 0.1)	ρ_{bulk} , g/cm^3 (± 0.001)	Porosity, % (± 0.01)
	a (\AA)	b (\AA)	c (\AA)			
$x = 0.00$	5.433	6.369	5.844	203.6	5.707	19.34
$x = 0.05$	5.437	6.373	5.871	203.7	5.778	18.57
$x = 0.10$	5.442	6.377	5.875	203.9	5.848	17.84

3.2 Atomic Force Microscopy measurements

The magnetic topology images of the $\text{Nd}_{0.75}\text{Na}_{0.25-x}\text{K}_x\text{MnO}_3$ manganite samples ($x = 0, 0.05,$ and 0.10) was generate using Atomic Force Microscopy (Bruker) with lift mode enabled at a scanning rate

of 0.5 Hz and varying tapping phases (scanning range). The Atomic Force Microscopy images revealed the magnetic domain regions of the manganite samples and magnetic topology anomaly images was generated using NanoScope Analysis 1.7 software.

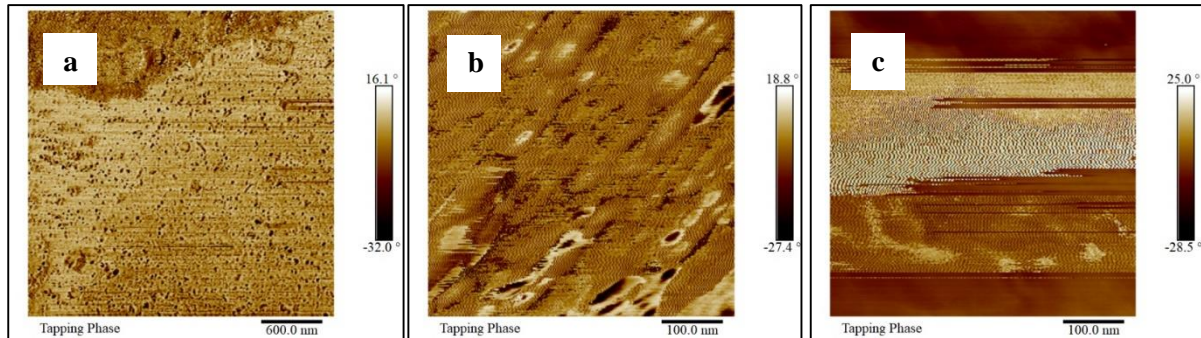


Figure 2: The magnetic domain region and magnetic topology anomaly images of sample $x = 0$ at a varying tapping phase (scanning range) which are a) 600.0 nm, b) 100.0nm, and c) 100.0 nm.

Figure 2 illustrates the magnetic domain region and magnetic topology anomaly images of sample $x = 0$ at a varying tapping phase (scanning range) which are a) 600.0 nm, b) 100.0nm, and c) 100.0 nm respectively. The topographic image in Figure 2 a) shows tapping phase area of 600.0 nm x 600.0 nm. Notably, a rough surface was observed and there was no magnetic domains detected in this specific area. However, a maze-like pattern was observed in the topographic image of Figure 2 b) and c) provide both tapping phases area of 100.0 nm x 100.0 nm which clearly exhibits the magnetic domains.

In addition, Figure 3 depicts the magnetic domain region and magnetic topology anomaly images of sample $x = 0.05$ at a varying of tapping phase (scanning range) which are a) 2.0 μm , b) 600.0nm, and c) 200.0 nm respectively. The topographic image in Figure 3 a) shows tapping phase area of 2.0 μm x 2.0 μm . Notably, a rough and an uneven surface was observed. However, there was no magnetic domains detected in this specific area. Significantly, in the topographic image of Figure 3 b) and c) provide tapping phases area of 600.0 nm x 600.0 nm and 200.0 nm x 200.0 nm a maze-like pattern was observed which clearly indicates the magnetic domains of sample $x = 0.05$.

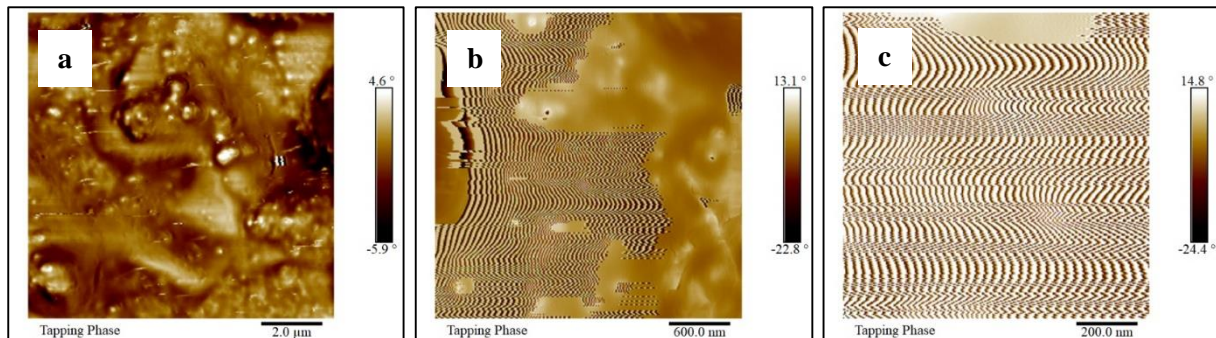


Figure 3: The magnetic domain region and magnetic topology anomaly images of sample $x = 0.05$ at a varying tapping phase (scanning range) which are a) 2.0 μm , b) 600.0nm, and c) 200.0 nm.

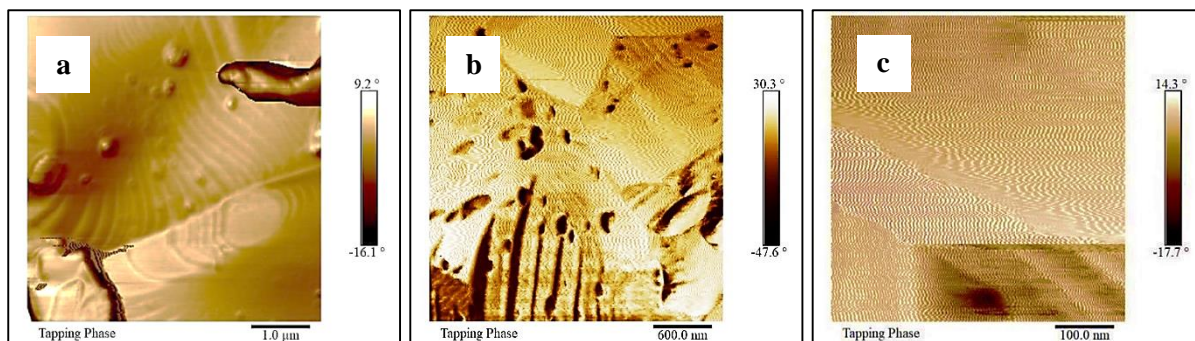


Figure 4: The magnetic domain region and magnetic topology anomaly images of sample $x = 0.10$ at a varying tapping phase (scanning range) which are a) $1.0 \mu\text{m}$, b) 600.0nm , and c) 100.0nm .

Moreover, Figure 4 portrays the magnetic domain region and magnetic topology anomaly images of sample $x = 0.10$ at a varying of tapping phase (scanning range) which are a) $1.0 \mu\text{m}$, b) 600.0nm , and c) 100.0nm respectively. Notably, a smooth and an uneven surface was observed in the topographic image shown in Figure 4 a) provide tapping phase area of $1.0 \mu\text{m} \times 1.0 \mu\text{m}$. However, there was no magnetic domains detected in this specific area. Significantly, in the topographic image of Figure 4 b) and c) provide tapping phases area of $600.0 \text{nm} \times 600.0 \text{nm}$ and $100.0 \text{nm} \times 100.0 \text{nm}$ a maze-like pattern was observed which clearly indicates the magnetic domains of sample $x = 0.10$. Furthermore, topographic image in Figure 4 c) has an even magnetic domains separation at certain sections of the image than that of in Figure 4 b).

Based on Figures 2,3, and 4, the element substitution of K ($x = 0, 0.05, \text{ and } 0.10$) to the $\text{Nd}_{0.75}\text{Na}_{0.25-x}\text{K}_x\text{MnO}_3$ manganite system was successful as it contributed towards the change in the magnetic domains and magnetic topology anomaly varying at different tapping phases (scanning area) of all the samples. The spectral root mean square (RMS) amplitude for all the samples ($x = 0, 0.05, \text{ and } 0.10$) varies for each of the magnetic topology images that was generated. The tabulation of the spectral root mean square (RMS) amplitude is as shown in Table 2,3 and 4.

Table 2: The tabulation of the spectral root mean square (RMS) amplitude and the topographic image of sample $x = 0$.

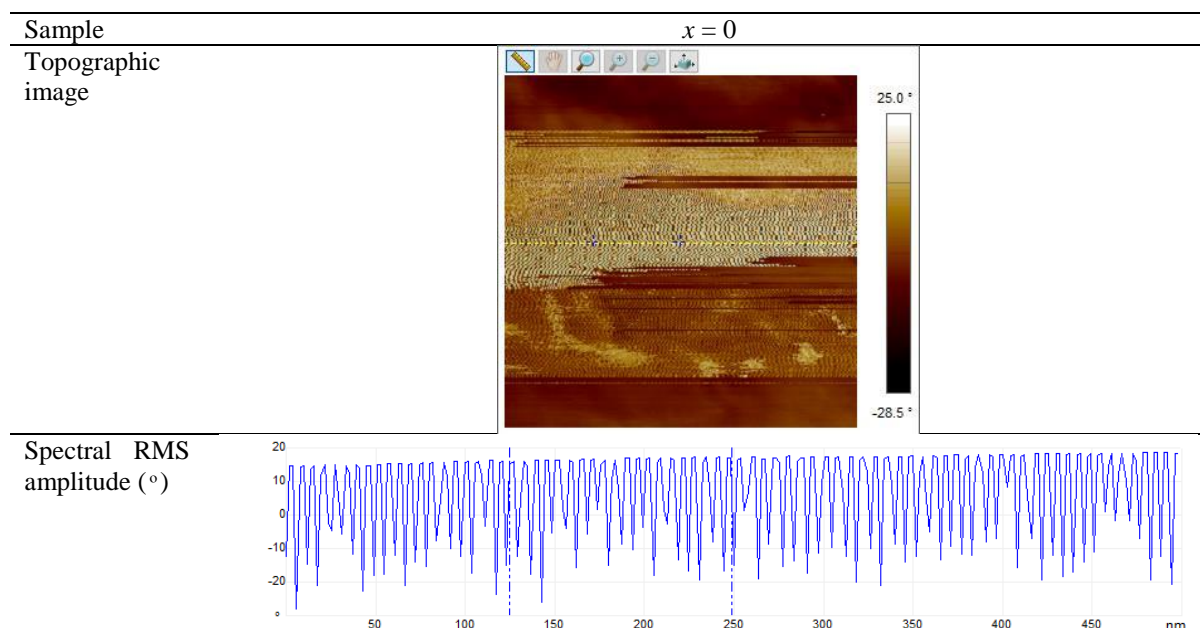


Table 3: The tabulation of the spectral root mean square (RMS) amplitude and the topographic image of sample $x = 0.05$.

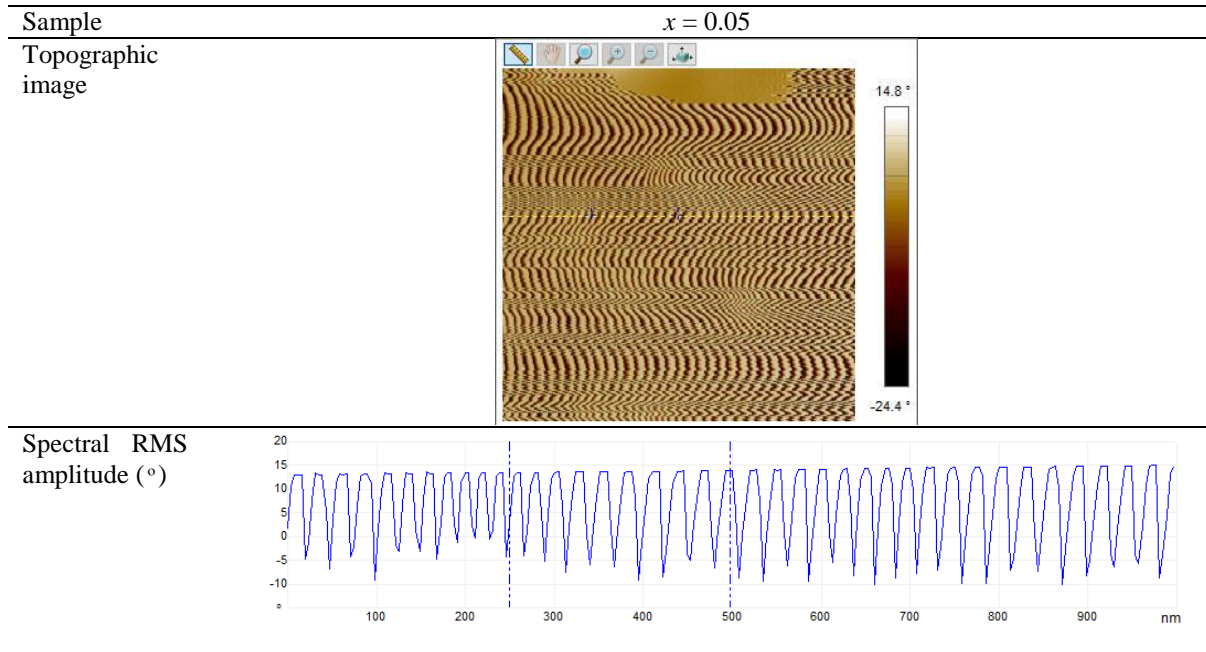
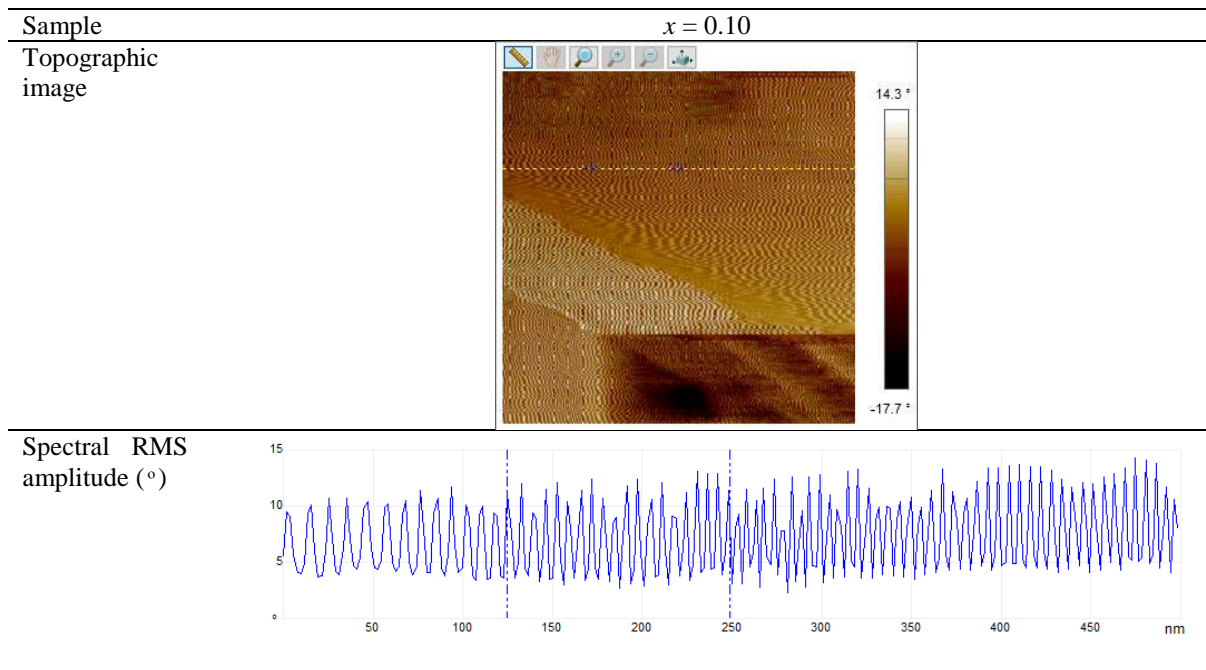


Table 4: The tabulation of the spectral root mean square (RMS) amplitude and the topographic image of sample $x = 0.10$.



Based on the data tabulated in Table 2, Table 3, and Table 4, there were observable changes in the spectral RMS amplitude of each samples ($x = 0, 0.05$, and 0.10) for all the sections showing a successful replacement of K^+ ions to the $Nd_{0.75}Na_{0.25-x}K_xMnO_3$ manganite oxide. Moreover, it can be clearly seen that the values of spectral RMS amplitude for samples ($x = 0.05$ and 0.10) did experience a systematically trend as the increase in K content which was 9.78° for sample $x = 0$, 9.95° for $x = 0.05$, and 10.1° for $x = 0.10$. The ideal magnetic domain was detected for the sample $x = 0.05$ as it showed smooth spectral RMS amplitude graph compared to $x = 0$ and $x = 0.10$. Thus, this result was congruent

with the result of XRD where the increasing in unit cell volume and bulk density contributed to the increase of the spectral RMS amplitude with significant trend for all of the samples.

4. Conclusion

In conclusion, there was a correlation noticed between XRD and AFM. The K substitution contributed to the changes in the unit cell volume, bulk density, porosity, magnetic topology and spectral RMS amplitude of the manganite sample. The modest rise in the unit cell volume (V), bulk density (ρ_{bulk}) contributed to the increase of the spectral RMS amplitude with significant trend and changes in magnetic topology for all of the samples with the K content. Thus, this shows a successful replacement of K^+ ions to the $\text{Nd}_{0.75}\text{Na}_{0.25-x}\text{K}_x\text{MnO}_3$ manganite oxide and this result was congruent with the result of XRD and AFM. As a whole of this study, it focused more on the structural properties, and magnetic topology of $\text{Nd}_{0.75}\text{Na}_{0.25-x}\text{K}_x\text{MnO}_3$ as mentioned in the previous objective. As to achieve better research study, few improvements and recommendations could be implemented by next researcher. The next researcher can proceed this research in detail on surface morphology and electrical transport properties with dissimilar substitution element such as monovalent or divalent element whether on Mn-site substitution. In this study it focused more on the investigation of monovalent doping agent on the Na-site of manganite compound and as for the difference, future researcher can conduct a study on substitution of transition-metal element on Mn-site of the $\text{Nd}_{0.75}\text{Na}_{0.25-x}\text{K}_x\text{MnO}_3$ manganite. Substitution of small amount of transition-metal element on the Mn sites has well influence on the charge ordering state [12].

Acknowledgement

This research was supported by TIER 1 Vot H967 Research Grant from Universiti Tun Hussein Onn Malaysia. Thanks to Ceramic and Amorphous Group, Faculty of Applied Sciences and Technology, Pagoh Higher Education Hub, Universiti Tun Hussein Onn Malaysia, 84600 Pagoh, Johor.

References

- [1] S. Kansara, D. Dhruv, B. Kataria, C. Thaker, S. Rayaprol, C. Prajapat, M. Singh, P. Solanki, D. Kuberkar, and N. Shah, "Structural, transport and magnetic properties of monovalent doped $\text{La}_{1-x}\text{Na}_x\text{MnO}_3$ manganites", *Ceramics International*, vol. 41, no. 5, pp. 7162-7173, 2015.
- [2] P. Thamilmaran, M. Arunachalam, S. Sankarajan, K. Sakthipandi, E. Samuel and M. Sivabharathy, "Study of the effect of Cu doping in $\text{La}_{0.7}\text{Sr}_{0.3}\text{MnO}_3$ perovskite materials employing on-line ultrasonic measurements", 2022.
- [3] M. Salamon and M. Jaime, "The physics of manganites: Structure and transport", *Reviews of Modern Physics*, vol. 73, no. 3, pp. 583-628, 2001.
- [4] Z. Li, X. Zhang, J. Yu, X. Liu, X. Liu, H. Liu, P. Wu, H. Bai, C. Sun, J. Lin, and E. Jiang, "Competition between the charge ordered and ferromagnetic states in $(\text{La,Nd})_{0.75}\text{Na}_{0.25}\text{MnO}_3$ manganites", *Physics Letters A*, vol. 325, no. 5-6, pp. 430-434, 2004.
- [5] S. Razali, N. Ibrahim, S. Shamsuddin and M. Noh, "Observation of Charge Ordering Signal in Monovalent Doped $\text{Nd}_{0.75}\text{Na}_{0.25-x}\text{K}_x\text{MnO}_3$ ($0 \leq x \leq 0.10$) Manganites", *International Journal of Engineering & Technology*, vol. 7, no. 430, p. 85, 2018.
- [6] S. Taran and H. Yang, "A comparative study of transport behaviour of monovalent (Li^+) and trivalent (Bi^{3+}) doped $\text{La}_{1-x}\text{Li}_x\text{MnO}_{3+\delta}$ and $\text{La}_{0.67-y}\text{Bi}_y\text{Ca}_{0.33}\text{MnO}_3$ CMR materials", *Materials Research Innovations*, vol. 24, no. 5, pp. 301-308, 2019.

- [7] C. Larsen, S. Samothrakitis, A. Fortes, A. Ayaş, M. Akyol, A. Ekicibil, and M. Laver, "Basal plane ferromagnetism in the rhombohedral manganite $\text{La}_{0.85}\text{Ag}_{0.15}\text{MnO}_{3+\delta}$ ", *Journal of Magnetism and Magnetic Materials*, vol. 498, p. 166192, 2020.
- [8] S. Shamsuddin, S. Supardan, A. Ibrahim and A. Yahya, "Ultrasonic Anomaly Near the Charge Ordering Transition in Sr-Doped $\text{Nd}_{0.3}\text{La}_{0.2}\text{Ca}_{0.5-x}\text{Sr}_x\text{MnO}_3$ Manganites", *Journal of Superconductivity and Novel Magnetism*, vol. 27, no. 5, pp. 1229-1234, 2013.
- [9] A. Modi, M. A. Bhat, D. K. Pandey, Tarachand, S. Bhattacharya, N. Gaur, and G. Okram, "Structural, magnetotransport and thermal properties of Sm substituted $\text{La}_{0.7-x}\text{Sm}_x\text{Ba}_{0.3}\text{MnO}_3$ ($0 \leq x \leq 0.2$) manganites", *Journal of Magnetism and Magnetic Materials*, vol. 424, pp. 459-466, 2017.
- [10] R. Thaljaoui, K. Pękała, M. Pękała, W. Boujelben, J. Szydłowska, J. Fagnard, P. Vanderbenden, and A. Cheikhrouhou, "Magnetic susceptibility and electron magnetic resonance study of monovalent potassium doped manganites $\text{Pr}_{0.6}\text{Sr}_{0.4-x}\text{K}_x\text{MnO}_3$ ", *Journal of Alloys and Compounds*, vol. 580, pp. 137-142, 2013.
- [11] J. Fan, L. Pi, K. He, W. Wang and Y. Zhang, "Charge ordering melting and evidence for a metastable antiferromagnetic phase in $\text{Nd}_{0.5(1-x)}\text{Ca}_{0.5(1+x)}\text{Mn}_{1-x}\text{Ti}_x\text{O}_3$ ", *Europhysics Letters (EPL)*, vol. 74, no. 3, pp. 506-511, 2006.
- [12] C. Xing, H. Zhang, K. Long, Y. Xiao, H. Zhang, Z. Qiu, D. He, X. Liu, Y. Zhang, and Y. Long, "The Effect of Different Atomic Substitution at Mn Site on Magnetocaloric Effect in $\text{Ni}_{50}\text{Mn}_{35}\text{Co}_2\text{Sn}_{13}$ Alloy", *Crystals*, vol. 8, no. 8, p. 329, 2018.